High-resolution continuum source graphite furnace molecular absorption spectrometry for the monitoring of Sr isotopes *via* SrF formation. A case study

A. Bazo,[1] R. Garde,[1] E. Garcia-Ruiz,[1] M. Aramendía,[1,2] F.V. Nakadi,[1] and M. Resano[1]*

[1]Department of Analytical Chemistry, Aragón Institute of Engineering Research (I3A), University of Zaragoza, Pedro Cerbuna 12, 50009, Zaragoza, Spain. E-mail: mresano@unizar.es

[2]Centro Universitario de la Defensa de Zaragoza, Carretera de Huesca s/n, 50090, Zaragoza, Spain

Abstract

High-resolution continuous source graphite furnace molecular absorption spectrometry (HR CS GFMAS) can provide isotopic information under certain conditions, thus broadening its field of application. However, up to date, only elements with two major stable isotopes have been monitored *via* this technique. In this work, the possibilities of HR CS GFMAS to determine isotope ratios of elements with more than two stable isotopes are evaluated for the first time. For this purpose, Sr was chosen as the analyte and SrF as the target species, so four different signals corresponding to the four stable Sr isotopes (^{88}Sr, ^{87}Sr, ^{86}Sr and ^{84}Sr) should be distinguished. Nevertheless, due to the number of strontium isotopes, the shape of the peaks, and the resolution that the instrument exhibits in the spectral window, isotopic signals overlap, thus leading to potentially biased results. To circumvent this issue, a deconvolution protocol, consisting of measuring and correcting for the contribution of each isotope on the signal of the

rest, was developed. These contributions were calculated as the signal ratio between the absorbance of the monoisotopic profile at the wavelengths where the maxima of other isotopes are expected, and at its own maximum. Therefore, the interference can be simply subtracted from the net signal registered for the interfered isotope. The performance of this method was demonstrated for both naturally abundant and isotope-enriched Sr standards, paving the way for future applications in this field. Analysis of real sample (tap water) spiked with a 84Sr solution is also demonstrated.

1. Introduction

Isotopic analysis consists of the measurement of the relative abundances (*i.e.*, the ratio of the abundance of a particular isotope to the total element) or isotope ratios (*i.e.*, the quotient between the concentration of two isotopes) of the different isotopes of an element in a given sample. These abundances are *a priori* constant in nature, but they can be altered by both natural and anthropogenic phenomena.[1] Therefore, isotopic analysis shows applications in very diverse areas such as forensic analysis,[2] geographical tracing,[3] dating applications,[4] tracer experiments,[5] migration studies,[6] etc. Generally, these analyses are carried out with dedicated instruments based on mass spectrometry (MS), which stand out for their high sensitivity and selectivity.[1]

In particular, the application of inductively coupled plasma mass spectrometry (ICP-MS) to this field needs to be highlighted, as this technique enables getting access to isotopic information for a large number of elements at trace and ultra-trace levels, thus offering very relevant data for all the scientific fields previously discussed,[7] but also when only elemental information is aimed at, either in real samples[8] or for the certification of reference materials,[9] *via* isotope dilution. When high-precision isotopic information is required (*e.g.*, for monitoring isotopic variations involving non-radiogenic nuclides), the use multi collector ICP-MS devices is typically needed.[10]

Given the multiple applications of isotope measurements, efforts have been devoted to find ways to get access to such type of information using other existing, less sophisticated techniques, based on optical spectrometry. The so-called laser ablation molecular isotopic spectrometry (LAMIS), albeit not very sensitive, is a perfect example of this,[11] enabling direct sample analysis. The use

of absorption spectrometry can also potentially lead to the development of fast and simple methodologies, and it is potentially more sensitive than other optical approaches.[12]

The theoretical principle enabling isotopic analysis in absorption/emission techniques is based on the isotopic shift, *i.e.*, the wavelength displacement that the signal of two isotopes of the same element display in the spectrum as a consequence of the slight variations in their energy levels. These shifts may *a priori* enable the evaluation of the signal of each isotope separately. However, they are expected to be minimal, so the use of high-resolution spectrometers is often necessary. Even then, the energy differences observed for atomic transitions of different isotopes are normally so small that the number of practical applications based on atomic spectrometry is limited to isotope ratios of light atoms, such as boron[13] or lithium,[14,15] or else of heavy ones that show a difference of various mass units.[16,17]

Alternatively, the use of molecular spectra opens new possibilities in this field, as demonstrated *via* LAMIS.[18] Molecules, unlike atoms, possess vibrational and rotational levels, which are much more affected by the mass nuclei than electronic levels, which are mainly governed by Coulombic forces.[11]

Nowadays, high-resolution continuum source spectrometers offer unmatched capabilities for measuring absorption in comparison with traditional line sources. In particular, they offer potential to monitor molecular spectra (normally originating from diatomic molecules in gas phase) with resolution down to almost 1 pm (depending on the wavelengths), possibilities for correcting for spectral interferences, and low detection limits, providing a graphite furnace that is used as vaporizer.[19–22] As a consequence, this technique, so-called high-resolution

continuous source graphite furnace molecular absorption spectrometry (HR CS GFMAS), has begun to be evaluated for isotopic analysis.

The first two works investigating this aspect were published by our research group and reported on the separate monitoring of $Al^{35}Cl$ and $Al^{37}Cl$ signals,[12] and those of $Ca^{79}Br$ and $Ca^{81}Br$,[23] respectively. Later, isotopic analysis of B, as ^{10}BH and ^{11}BH was also demonstrated by Abad *et al*.[24] Finally, the quantification of ^{40}Ca and ^{44}Ca, using ^{40}CaF and ^{44}CaF, has been recently reported as well.[25] In all these cases, only two isotopes were monitored or ratioed.

The aim of the present work is to proceed one step further and evaluate, for the first time, the possibilities of the technique to determine isotope ratios in cases when more than two sufficiently abundant and stable isotopes are present. For this purpose, Sr is an ideal target, as it exhibits four stable isotopes of different abundance in nature: 0.8258 ^{88}Sr, 0.0700 ^{87}Sr, 0.0986 ^{86}Sr, and 0.0056 ^{84}Sr (values given as mol fractions).[26] Moreover, ^{87}Sr is of special interest given its radiogenic nature, *i.e.,* its generation by the radioactive decay of ^{87}Rb nuclei through the emission of β^- particles,[1] that enables many applications such as dating,[27] provenance studies of food and other samples,[1] or migratory studies,[28] among others. The rest of isotopes have also been monitored and have found applications in archaeology,[29] geochemistry,[30] environmental sciences,[31] and chemostratigraphy,[32] to mention a few.

The best conditions for the formation of SrF in the graphite furnace will be discussed. Moreover, suitable strategies for the accurate monitoring of the different Sr isotopes, based on deconvolution, will be introduced.

2. Experimental

2.1. Reagents, standards, and samples

Reagents of analytical purity grade were used for all experiments. Deionized water (18 MΩ cm) obtained from a Milli-Q water system (Millipore, France) was used throughout the work. A 1000 mg L^{-1} Sr stock standard (Merck, Germany) was used to prepare natural isotope composition strontium solutions. For Sr isotope measurements, ^{88}Sr, ^{87}Sr (both from Cortecnet, France), ^{86}Sr (SPEX CertiPrep, USA) and ^{84}Sr (Neonest AB, Sweden) enriched carbonates (as the solid) were used. The atomic composition (in %) of each Sr carbonate is presented in **Table 1**. As fluorinating agents, a 1% v/v methyl fluoride-argon mixture (Ar/CH_3F, Nippon Gases, Spain), 99% sodium fluoride (Panreac, Spain) and 99.9% ammonium bifluoride (Sigma Aldrich, USA) were used. Finally, a 2% v/v hydrogen-argon mixture (Ar/H_2, Nippon Gases) was selected as purge gas.

For the tracer experiment described in section 3.5., tap water collected in our laboratory was used as real sample and spiked with the ^{84}Sr solution mentioned above.

2.2. Instrumentation

Measurements were performed with a ContrAA 800G high-resolution continuum source atomic absorption spectrometer (Analytik Jena AG, Germany), using transversally-heated graphite tube atomizers that incorporate a platform (Analytik Jena AG). Regarding sample introduction, an autosampler ASGF (Analytik Jena AG) was deployed for automatic pipetting.

For validation purposes, a NEXION 300X ICP mass spectrometer (Perkin Elmer, USA) was deployed, using the following parameters: nebulizer Ar flow 1.1

L min^{-1}, auxiliary Ar flow 1.2 L min^{-1}, plasma Ar flow 15 L min^{-1}, and ICP radiofrequency power 1450 W. Samples were analyzed with a dwell time of 50 ms, monitoring ^{88}Sr for the determination of total Sr, while for the tracer experiment ^{84}Sr and ^{88}Sr were measured.

2.3. Measurement protocol for isotopic analysis

Unless otherwise noted, solutions were analyzed in quintuplicate, using the temperature program shown in **Table 2**. Strontium monofluoride (SrF) was the molecule monitored, *via* its $X^2\Sigma^+ \rightarrow A^2\Pi$ (0,1) vibronic transition,[33] which rendered seven evenly spaced double-headed bands within the spectral window (629.817 nm – 630.718 nm), as shown in **Figure 1**. However, this study has focused on the most sensitive band only, which was found to show its maximum at 630.341 nm for ^{88}SrF. As it is common in methods developed for isotope analysis with HR CS GFMAS, signals were evaluated in terms of peak height, considering only one pixel (that of the maximum),[12] unless otherwise indicated. The IBC-m mode for background correction was selected, and the signal smooth setting was set to weak (default software option).

3. Results and discussion

3.1. Choice of molecule-forming conditions for Sr isotope analysis

First, the fundamentals of the approach intended need to be reminded. The basic strategy here consists in forming a diatomic molecule containing the analyte, as in this way more transitions but, above all, a much larger isotopic shift in comparison with those observed for atomic lines will be obtained. This shift responds to the theoretical equation proposed by Herzberg,[34] given below, so it can be calculated *a priori* for different molecules:

$$\Delta\upsilon = (1-\rho)\left[\omega'_e\left(\upsilon'+\frac{1}{2}\right)-\omega''_e\left(\upsilon''+\frac{1}{2}\right)\right]-(1-\rho^2)\left[\omega'_e x'_e\left(\upsilon'+\frac{1}{2}\right)^2-\omega''_e x''_e\left(\upsilon''+\frac{1}{2}\right)^2\right] + (1-\rho^3)\left[\omega'_e y'_e\left(\upsilon'+\frac{1}{2}\right)^3-\omega''_e y''_e\left(\upsilon''+\frac{1}{2}\right)^3\right] \quad (1)$$

Where $\Delta\upsilon$ is the theoretical isotopic shift in cm^{-1}, υ is the vibrational quantum number, ω_e is the harmonic frequency, x_e and y_e are the first and second anharmonic constants, and ρ stands for $(\mu/\mu^i)^{1/2}$, μ and μ^i being the reduced mass of the molecule with the lighter and heavier isotope, respectively. Apostrophes distinguish between the two electronic levels involved in the transition: one single apostrophe for the upper level and two for the lower one. The number of terms is theoretically infinite, but as discussed by Nakadi *et al.*, using only three suffices for good agreement with the experimental shifts.[12]

From equation (1) it follows that those transitions involving a greater variation between quantum numbers, starting from higher vibrational levels, will also show larger isotopic shifts. Unfortunately, these transitions are not usually the most sensitive ones, since, even at the high temperatures reached by conventional atomizers, the fundamental level is still the most populated one. Therefore, there is always a trade-off between achieving sufficient sensitivity and a large enough isotopic shift, such that a suitable balance needs to be found.

Second, when selecting an adequate target molecule, it is of the utmost importance to achieve simple and sensitive spectra, as not every molecule will show the same sensitivity and number of transitions. In this sense, strontium monofluoride (SrF) is proposed as an appropriate candidate for the strontium isotope determination given its high bonding energy (538.48 kJ mol^{-1}),[35] which

guarantees the stability of the molecule at the high temperatures reached inside the graphite chamber.[36–38] Moreover, the use of this molecule minimizes the risk of suffering from chemical interferences caused by competition of fluorine with other species that might be present in any sample, as all other Sr diatomic molecules show lower bonding energies than SrF (426 kJ mol^{-1}, corresponding to SrO, or below).[39] Additionally, fluorine is a monoisotopic element, which in turn leads to simpler molecular spectra, where every shift can actually be attributed to a particular Sr isotope. This latter factor is especially important in the current case, since the spectrum is expected to be complex enough already, as Sr possesses four relatively abundant isotopes in nature. The spectra of the SrF molecule ($X^2\Sigma^+ \rightarrow A^2\Pi$ (0,1) vibronic transition) in the region of 630 nm is shown in **Figure 1**.

Third, different fluorinating agents were tested to promote the formation of the SrF target molecule. Two different fluorination approaches were evaluated: (i) NaF and $NH_4F{\cdot}HF$ were added as aqueous solutions together with the Sr aqueous standard in the graphite furnace; and (ii) an argon-methyl fluoride mixture (Ar/CH_3F) was added in the gas phase during the graphite furnace temperature program. In fact, it has been described in the literature that the main mechanism through which SrF is formed in the graphite furnace is *via* the gas phase recombination of Sr and F atoms,[40] so testing a gas-phase fluorinating agent was considered worthy. The use of gas phase for addition of the reagent was also satisfactorily reported by Abad *et al.* for the formation of BH.[24] For these fluorination tests, 10 µL of a 100 µg L^{-1} Sr solution (1 ng Sr) were introduced into the graphite furnace.

As for the temperature program, a conventional program was first tested for the aqueous fluorinating agents, which were added as 5% (m/m) solutions (10 µL). No SrF signal could be registered for NaF at any combination of pyrolysis/vaporization temperatures, although this fluorinating agent had been reported to succeed in generating the calcium monofluoride molecule in the graphite furnace (CaF).[25] On the contrary, addition of $NH_4F{\cdot}HF$ (a fluorinating agent that performed satisfactorily in previous works)[41] succeeded in generating the SrF molecule. A basic optimization of the pyrolysis and vaporization temperatures was next carried out. Results when monitoring the most sensitive transition, which is reported to be found at 651.187 nm,[42] are shown in **Figure 2**. A somewhat stable signal was obtained for a pyrolysis temperature of up to 1100 ºC, so 800 ºC (low enough to prevent any potential analyte losses) was selected for the further development of the method. As for the vaporization, a plateau was reached for temperatures over 2300 ºC, so 2400 ºC was selected to assure the highest sensitivity and still maximize the lifetime of the graphite components. The optimized temperature program finally selected is shown in **Table S1** in the Electronic Supplementary Information (ESI).

Next, fluorination in the gas phase was intended by introduction of the Ar/CH_3F gas mixture through the additional gas channel of the instrument during the gas adaptation and vaporization stages of the temperature program. The additional gas channel flow was set at 0.5 L min^{-1} as this is the only possible value allowed by the software. Although the SrF molecule was formed with this fluorinating agent and a signal could be registered, the sensitivity achieved was significantly lower than that obtained with aqueous solutions of $NH_4F{\cdot}HF$. This fact could be anticipated due to the enhanced diffusion of the SrF molecule

outside the graphite furnace produced by the relatively high flow rate maintained during the vaporization stage.

To circumvent this issue, an adapted temperature program was developed with the idea of loading the graphite furnace with the Ar/CH_3F reactive gas mixture just before the onset of the vaporization step, during which all internal gas flows were stopped to increase the residence time of the SrF molecule inside the furnace and, thus, enhance the analytical signal. The adapted temperature program is shown in **Table 2**. Please notice that there are some software limitations in the way in which the program settings can be introduced, so it is necessary to use terms and conditions that can be accepted by this software. The exact software settings used to set the temperature program described in **Table 2** are provided as ESI (**Table S2**). With this new temperature program, the sensitivity achieved with the Ar/CH_3F gas mixture improved significantly, to the point where it was better than that obtained for $NH_4F{\cdot}HF$, as shown in **Figure 3A**.

As a final optimization test, the purge gas was changed from argon to an Ar/H_2 gas mixture which, due to a more reducing environment, may facilitate the formation of the atoms in gas phase.[40] In any case, this approach leads to an additional improvement in sensitivity by approximately a 30%, as shown in **Figure 3B**.

To sum up, the methodology that was found to be optimal for the formation of SrF in the graphite furnace and for the measurement of its absorbance consisted of the use of an Ar/CH_3F gas mixture as fluorinating agent and an Ar/H_2 mixture as purge gas, with a temperature program optimized to maximize the formation and the residence time of SrF inside the graphite furnace.

3.2. Choice of wavelength for isotope measurements

As previously discussed, there is an inverse relation between the sensitivity of a transition and the expected isotopic shift, as predicted by equation (1). As a result, the most sensitive transition, which was monitored for signal optimizations in the previous section, was found to be not suitable for isotope analysis purposes. At this wavelength, the shift is too small ($\Delta\lambda_{theoretical}$ = 0.12 pm) to be measured with the resolution of our instrument (4.4 pm/pixel at 651.2 nm), and thus, a compounded Sr signal (sum of all four stable isotopes) is recorded. Consequently, other SrF transitions[33,43] that, according to equation (1), are expected to exhibit isotopic shifts that can be observed with the resolution of the instrument (pm level) were evaluated, searching for a region were the sensitivity is high enough for quantitative analysis. For this purpose, 0.1 µg of naturally abundant Sr was measured at the different SrF transitions shown in **Table 3,** where each characteristic mass, *i.e.*, the Sr mass that is expected to render an absorbance of 0.0044 at the maximum of the transition if linear behavior is assumed, is also displayed. For informative purposes on the selection of the best suited lines for isotopic analyses, the resolution of the spectrometer at each of the transitions is also displayed in **Table 3**.

In short, only four of the tested transitions exhibited enough sensitivity to render peaks distinguishable from the background. Even though transitions at 630.34 and 641.76 nm show a much larger shift than those at 372.16 and 364.10 nm, in practice, it needs to be reminded that the resolution of the instrument varies with the wavelength, being lower at higher wavelengths as shown in **Table 3** (2.6 pm/pixel at 360 nm and 4.6 pm/pixel at 630 nm). Still, shift differences are substantial enough to justify discarding the shorter wavelength transitions (*e.g.*,

9 pixels at 630.34 nm and 6 pixels at 364.10 nm for the ^{86}Sr-^{88}Sr shift, see **Table 3**). Among, the two remaining transitions, the one at 630.34 nm offers superior sensitivity and was therefore selected for the further development of the method.

Moreover, in this region a series of seven distinct peaks of variable sensitivity can be observed within the spectral window. These peaks correspond to different rotational levels within the same vibronic transition, so they are expected to exhibit similar isotopic shifts, as the impact of rotational terms on the isotopic displacement is negligible. Thus, in case of need (*e.g.,* occurrence of spectral interferences), it is possible to monitor any of them as convenient, but for this work we will focus on the most sensitive peak, which shows the maximum at 630.34 nm.

Once the optimal transition has been selected, it is important to emphasize that, despite trying to maximize both sensitivity and isotopic shift, in a complicated case such as this one with 4 stable isotopes, and not only 2, the shift may still be insufficient to achieve fully resolved signals enabling individual isotope quantification in a straightforward manner. Therefore, depending on both the shift and the peak profile, signal deconvolutions may be necessary to circumvent the effect of spectral overlaps.

To portrait the magnitude of such overlaps in this case, isotope-enriched solutions prepared from their respective standards (see **Table 1** for their isotopic composition) at a concentration of 10 mg L^{-1} of total strontium were measured, leading to the spectra collected in **Figure 4A**. From these spectra it is possible to conclude that isotopic peaks for a given transition spread over lower wavelengths, leading to spectral overlaps that, given the summative nature of absorbance, would entail isotope misestimations, unless corrected. Therefore, correction

strategies are mandatory to subtract the contribution that each isotope shows on the signal at the maxima of the rest.

By collecting these spectra, and besides assessing the existence of spectral overlaps, the exact wavelength position of the maximum signal for the different isotopes could also be determined and it is shown in **Figure 4B**. In this sense, and according to information on **Table 1**, it can be noticed that all isotopic standards used in the study contain a significant amount of ^{88}Sr, the most abundant in nature. Since the ^{84}Sr standard is the less pure of them all, a second maximum corresponding to ^{88}SrF can also be clearly appreciated in **Figure 4B** when this standard was measured.

3.3. Corrections for spectral overlap

For spectral correction, mathematically deconvoluting the measured spectra into their monoisotopic peaks would be the ideal methodology to circumvent this kind of issue. Notwithstanding, it is not easy to achieve optimal results with this approach given the relatively small isotopic shifts observed, the elevated number of isotopes, and the great contrast between the natural abundance of ^{88}Sr and the rest of the isotopes, which hinders the obtention of accurately deconvoluted peaks for the less abundant isotopes. In any case, a correction method was developed based on subtracting the contribution of every interfering isotope from the experimental signal measured at the wavelength where the peak maximum for each isotope appears, using signal ratios calculated from their monoisotopic peak profiles and according to the following equation:

$$S_{i,\ \text{corrected}} = S_{i,\text{exp}} - \sum_{k} R_{k,i} S_{k,\text{corrected}} \qquad (2)$$

where i refers to the isotope whose signal is to be corrected, and k refers to every other Sr isotope that interferes with the signal of the isotope i. $S_{i,exp}$ is the experimental raw signal directly measured at the wavelength of the maximum for isotope i (λ_i, see **Figure 5**); $R_{k,i}$ is the ratio between the signal obtained for the isotope k at λ_i and at the wavelength of the maximum for isotope k (λ_k); and, finally, $S_{k,corrected}$ is the signal corrected (if needed) at λ_k.

According to equation (2), the first step is to identify, for every isotope, its interfering species (*i.e.*, isotopes that have a profile that exhibits a net signal distinguishable from the background at the wavelength where the maximum signal for another isotope appears). As observed in **Figure 4B**, the maximum for each isotope, indicated with dashed lines, only intersects with the peak profile of isotopes of higher mass and, thus, ^{88}SrF is practically not interfered by the signal of other isotopes, so its signal can be directly determined from the raw measurements.

It should be stressed again that the impossibility to obtain perfectly pure isotopic standards precludes the obtention of unimodal peaks for each isotope. Thus, even though ^{88}SrF seems to be overlapped by a shoulder of the ^{87}SrF profile, this effect is due to the presence of ^{88}Sr content in the isotope-enriched salt (8.4%, see **Table 1**) and not because of a real overlap with the signal originating from ^{87}Sr. Analogously, the ^{87}Sr and ^{88}Sr content in the ^{84}Sr enriched standard (2.0% and 18.1%, see **Table 1**) leads to the registration of secondary signals at the wavelengths corresponding to the maxima of such isotopes that do not actually belong to the ^{84}Sr profile. Moreover, it is also observed that ^{84}SrF is only significantly interfered by ^{86}SrF. In summary, ^{88}SrF is not significantly interfered by other isotopes; ^{87}SrF is only interfered by ^{88}SrF; ^{86}SrF is interfered

mostly by ^{87}SrF but also by ^{88}SrF; and ^{84}SrF is only significantly interfered by ^{86}SrF, as the ^{88}SrF and ^{87}SrF signals are shifted very far to the right of the spectrum.

After identifying the interfering species, the next step is to determine, for each isotope, the correction ratios of their interferences ($R_{k,i}$). The obtention of such ratios is *a priori* as simple as registering the spectrum of each isotope and measuring the quotient between the signal at the wavelengths where the maxima of interfered isotopes are expected and at its own maximum. However, given the significant impurities present in most of the isotope-enriched standards (see **Table 1**), this strategy is not practicable.

To circumvent this issue, an extrapolation method, described in **Figure 5**, was used. With this approach, the correction ratios for the interferences were measured for the ^{88}Sr enriched standard ($R_{k,88}$; see **Figure 5A**), which stands out because of its purity (99.9%), to be then extrapolated to the rest of isotopes (**Figure 5B**) so they can be used to correct the overlaps as schematized in **Figure 5C** and in accordance with equation (2). This extrapolation is based on the fact that the wavelength peak profiles for the monofluoride molecules of all the strontium isotopes are practically identical, only that they are shifted by a constant value per mass unit. In fact, roughly the same shifts were measured for the isotope pairs differing in one unit, ^{87}Sr-^{88}Sr and ^{86}Sr-^{87}Sr (20.1 and 20.7 pm, respectively), and for those differing in two units, ^{86}Sr-^{88}Sr and ^{84}Sr-^{86}Sr (40.8 and 40.7 pm, respectively). Therefore, the same correction ratios can be used for isotope pairs differing by the same number of mass units.

This presumption seems reasonable considering that the same transition is being registered for every isotope, and that the differences in terms of mass

are minor. Moreover, its validity can be confirmed in **Figure 6**, where the similarity in the shape of monoisotopic peaks, when normalized and overlayed, can be appreciated. In this figure, differences in the shape of the tail can be ascribed to isotopic impurities, which are especially evident for the ^{84}Sr enriched standard.

Therefore, to determine the experimental correction ratios ($R_{k,i}$), ^{88}Sr monoisotopic standard solutions between 0.24 and 1.2 mM with increments of 0.12 mM were measured, providing a value of 0.391 ± 0.014 for the $R_{88,87}$ and $R_{87,86}$ correction ratios, and 0.219 ± 0.008 for the $R_{88,86}$ and $R_{86,84}$ ratios (uncertainty expressed as standard deviation, n = 5). It is noteworthy that no dependence with concentration was observed for these experimental ratios; instead, the obtained values were distributed around a mean value as shown in **Figure 7**, which entails that the same correction ratios can be used for all the concentration range tested. Moreover, these ratios were calculated again after a two-month period and using a different graphite tube and platform, and still no significant difference was observed ($R_{88,87}$ = 0.401 ± 0.008 and $R_{87,86}$ = 0.223 ± 0.009), so the robustness of the correction is proven.

The limit of quantification (LOQ) was calculated with these measurements, and a value of 0.013 mM was obtained (for a sample volume of 10 µL, corresponding to 11.4 ng of ^{88}Sr). Similar measurements of the LOQ were performed for the rest of the isotopes, leading to values of 0.013 mM (11.3 ng), 0.012 mM (11.2 ng) and 0.014 mM (10.9 ng) for ^{87}Sr, ^{86}Sr and ^{84}Sr, respectively.

To evaluate the performance of the correction, different proportions of a 100 mg L^{-1} natural Sr standard solution and of standard solutions of similar concentrations but enriched in each of the minor Sr isotopes were introduced into the graphite furnace. Then, the absorbance ratio between each enriched isotope

and ^{88}Sr was calculated both before and after the correction. Given the fact that the sensitivity for the same transition is roughly identical for the different isotopes, plotting the measured absorbance ratio against the expected isotope ratio should ideally provide a line with a slope of 1 and an intercept of 0 if interferences were absent.

The results obtained are shown in **Figure 8**. A deviation from the expected results was particularly noticeable when working with the ^{87}Sr-enriched solution (an additive interference was observed because, in that particular case, the amount of ^{88}Sr remained fairly constant during the experiment) and with the ^{86}Sr-enriched solution. However, in all cases the correction led to results in good agreement with the expected values, for both the slope and the intercept, as shown in **Table 4**.

In summary, the signal ratios-based method has been proven to succeed in the correction of the overlaps for all the three minor strontium isotopes.

3.4. Analysis of standards containing multiple Sr isotopes

Once the method for Sr isotopic analysis was developed, its performance to simultaneously determine multiple isotope ratios in a single sample was investigated for 10 μL of strontium standards of natural abundance of 100 and 200 mg L^{-1} in total strontium. The reason for selecting these concentrations is that they result in levels above the limits of quantification for the three major isotopes. However, the determination of ^{84}Sr at this level is not practicable, since it is under the limit of quantification, and adding more natural strontium would result in both the saturation of the ^{88}Sr signal (*i.e.*, not in the linear range) and memory effects caused by the refractory nature of Sr. To compare the experimentally determined

isotope ratios with the theoretical abundances, Student's t-tests were performed, and the results collected in **Table 5**. These results confirm that the method succeeds in determining two different isotope ratios from a single measurement. Finally, to further prove the potential of the approach to determine multiple isotopes, monoisotopic standard solutions were diluted and mixed to achieve a concentration for each standard of 0.5 – 0.7 mM in total Sr so that the four Sr isotopes could be simultaneously determined. The registered spectrum for 20 µL of the new standard is shown in **Figure 9**, in which a maximum can be clearly observed for each isotope (in every one of the bands shown), and the results achieved are collected in **Table 6**. Student's t-tests confirmed that all the isotope ratios are in good agreement with the theoretical values, therefore demonstrating the capability of HR CS GFMAS to determine more than one isotope ratio from the same measurement.

3.5. Application of the methodology developed for the determination of ^{88}Sr and ^{84}Sr in a real sample

Obviously, the precision reported (6 – 11%) does not compete with that provided *via* dedicated MS techniques and will not suffice to study natural variations (*e.g.,* in nature, $^{87}Sr/^{88}Sr$ and $^{86}Sr/^{88}Sr$ isotope ratios range between 0.084 and 0.087, and 0.118 and 0.121,[17] respectively), but it could be sufficient for tracer experiments or for enabling the use of isotope dilution for calibration. On this topic, isotope analysis *via* HR CS GFMAS is still in its early stages, and the reason for the imprecision levels are not fully understood. In this particular case, the deconvolution approach needed to solve the complex spectra may play a significant role in this regard.

To further prove the potential of the approach for tracer experiments in which real samples are enriched in a given strontium isotope, tap water collected in our laboratory was spiked with the ^{84}Sr enriched standard until a concentration of about 60 mg L^{-1} for the main isotope was reached and, thus, it could be monitored as tracer. The selection of ^{84}Sr as tracer is due to two main reasons. First, it is the most resolved isotope, so the impact of spectral interferences from the matrix on the ^{84}Sr signal will be less significant. Second, it is the scarcest Sr isotope in nature, so the contribution of naturally present ^{84}Sr in the matrix is expected to be negligible, regardless of the concentration of natural Sr.

The sample was found to contain a concentration of 0.86 ± 0.02 mg L^{-1} of total Sr (concentration determined by ICP-MS before ^{84}Sr spiking), which is under the LOD of the SrF method, so the impact of naturally present strontium on the signals is negligible, as anticipated. Nevertheless, tap water is a sample containing many ions, which could translate into matrix effects (*e.g.*, as a consequence of the competition stablished between calcium and strontium for their fluorination). Therefore, to evaluate the impact of matrix effects, the concentration of both ^{84}Sr and ^{88}Sr in the spiked sample was determined and validated by comparing the results achieved with those obtained *via* ICP-MS, as shown in **Table 7**.

These results confirm that no significant matrix effects were found, as the methodology developed succeeds in the monitoring of ^{84}Sr for tracer studies, leading to concentration values not significantly different from those achieved by ICP-MS, using a straightforward calibration with aqueous standards.

Still, it is again clear that the precision values reached with both techniques are not comparable. In this sense, it should be remarked again that the goal of

this work at this point is not to try to compete with ICP-MS, but to study the possibilities of HR CS GFMAS for the simultaneous quantification of the four strontium isotopes.

4. Conclusions

This work explores for the first time the possibilities of HR CS GFMAS for isotope ratio monitoring of elements with more than two abundant isotopes, using Sr (through the formation of the SrF molecule) as proof of concept. Results confirm the potential of the technique, which is able to determine $^{87}Sr/^{88}Sr$ and $^{86}Sr/^{88}Sr$ ratios in naturally abundant Sr standards of concentration in total strontium above 100 mg L^{-1}, and also the $^{84}Sr/^{88}Sr$ ratio in spiked solutions. The major challenge faced during the development of the method was the need to correct for spectral overlap among the signals of the different isotopes themselves. In that regard, such predicament was circumvented by calculating signal ratios to subtract the contribution of the signals originating from heavier isotopes on those stemming from the lighter ones. Those applications requiring Sr isotope analysis in natural samples normally demand a precision that is currently beyond the possibilities of the current method, but it is also demonstrated that the method could be useful for tracer experiments, as proven by determining ^{84}Sr and ^{88}Sr in tap water. In any case, further work is needed to evaluate the main factors affecting the precision and possibilities to improve it.

Concerning the formation of the target molecule, the method was finely optimised to maximize the sensitivity, concluding that an Ar-CH_3F gas mixture is the best choice among the tested agents, especially in the presence of hydrogen in the purge gas. Finally, for data processing, only the most sensitive band (λ = 630.341 nm) of the spectral window monitored was considered since it minimises

the quantification limit down to 0.013 mM, when 10 µL of standard are introduced. Nevertheless, the rest of the bands could be also monitored, if required, to avoid the potential occurrence of spectral interferences in some matrixes.

Conflicts of interest

There are no conflicts of interest to declare

Acknowledgements

The authors are very grateful for the grants PGC2018-093753 – B-I00 and PID2021-122455NB-I00, funded by MCIN/AEI/10.13039/501100011033, and also acknowledge the funding received by the Aragon Government (Construyendo Europa desde Aragón, Grupo E43_20R).

References

1 F. Vanhaecke and K. Kyser, The Isotopic Composition of the Elements, in *Isotopic Analysis: Fundamentals and Applications Using ICP-MS*, eds. F. Vanhaecke and P. Degryse, Wiley-VCH, Weinheim, 1st edn, 2012, pp. 1–29.

2 M. Resano and F. Vanhaecke, Forensic Applications in *Isotopic Analysis: Fundamentals and Applications Using ICP-MS*, eds. F. Vanhaecke and P. Degryse, Wiley-VCH, Weinheim, 1st edn, 2012, pp. 391-418.

3 D. Rashmi, P. Shree and D. K. Singh, *Food Control*, 2017, **79**, 169-176.

4 M. A. Elburg, Geochronological Dating in *Isotopic Analysis: Fundamentals and Applications Using ICP-MS*, eds. F. Vanhaecke and P. Degryse, Wiley-VCH, Weinheim, 1st edn, 2012, pp. 235-274.

5 M. Montes-Bayón and J. Bettmer, The Use of Stable Isotopic Tracers in Metallomics Studies in Metallomics. Advances in Experimental Medicine and Biology, ed. M. Arruda, Springer, Cham, v. 1055 2018, pp. 111-137.

6 H. L. Whelton, J. Lewis, P. Halstead, V. Isaakidou, S. Triantaphyllou, V. Tzevelekidi, K. Kotsakis and R. P. Evershed, *J. Archeol. Sci. Rep.*, 2018, **20**, 768-774.

7 P. Penanes, A. Reguera-Galan, G. Huelga-Suarez, J. Rodríguez-Castrillón, M. Moldovan and J. Garcia Alonso, *J. Anal. At. Spectrom.*, 2022, **37**, 701-726.

8 C.L.S. Wiseman, A. Parnia, D. Chakravartty, J. Archbold, R. Copes and D. Cole, *Environ. Res.*, 2019, **169**, 261-271.

9 M. Sargent, H. Goenaga-Infante, K. Inagaki, L. Ma, J. Meija, A. Pramann, O. Rienitz, R. Sturgeon, J. Vogl, J. Wang and L. Yang, *Metrologia*, 2019, **56**, 034005.

10 M. Kirchenbaur, A. Heuser, A. Bragagni and F. Wombacher, *Geostand. Geoanalytical Res.*, 2018, **42**, 361-377.

11 A. A. Bol'shakov, X. Mao, J. J. González and R. E. Russo, *J. Anal. At. Spectrom.*, 2016, **31**, 119–134.

12 F. V. Nakadi, M. A. M. S. da Veiga, M. Aramendía, E. García-Ruiz and M. Resano, *J. Anal. At. Spectrom.*, 2015, **30**, 1531–1540.

13 H. Wiltsche, K. Prattes, M. Zischka and G. Knapp, *Spectrochim. Acta Part B*, 2009, **64**, 341–346.

14 A. Winckelmann, S. Nowak, S. Richter, S. Recknagel, J. Riedel, J. Vogl, U. Panne and C. Abad, *Anal. Chem.*, 2021, **93**, 10022–10030.

15 A. Winckelmann, D. Morcillo, S. Richter, S. Recknagel, J. Riedel, J. Vogl, U. Panne and C. Abad, *Anal. Bioanal. Chem.*, 2022, **414**, 251–256.

16 O. Zeiri, N. Fruchter, E. Elish, H. Gizbar, D. Shamir and I. Sedgi, *Anal. Chem.*, 2021, **93**, 5123–5128.

17 M. Krachler and R. Alvarez-Sarandes, *Microchem. J.*, 2016, **125**, 196–202.

18 R. E. Russo, A. A. Bol'shakov, X. Mao, C. P. McKay, D. L. Perry and O. Sorkhabi, *Spectrochim. Acta Part B*, 2011, **66**, 99–104.

19 B. Welz, H. Becker-Ross, S. Florek, U. Heitmann, *High-Resolution Continuum Source AAS: The Better Way to Do Atomic Absorption Spectrometry*, Wiley-VCH, Weinheim, 1st edn, 2005.

20 B. Welz, S. Morés, E. Carasek, M. G. R. Vale, M. Okruss and H. Becker-Ross, *Appl. Spectrosc. Rev.*, 2010, **45**, 327–354.

21 M. Resano, M. R. Flórez and E. García-Ruiz, *Spectrochim. Acta Part B*, 2013, **88**, 85–97.

22 M. Resano, E. García-Ruiz, M. Aramendía and M. A. Belarra, *J. Anal. At. Spectrom.*, 2019, **34**, 59–80.

23 F. V. Nakadi, M. A. M. S. da Veiga, M. Aramendía, E. García-Ruiz and M. Resano, *J. Anal. At. Spectrom.*, 2016, **31**, 1381–1390.

24 C. Abad, S. Florek, H. Becker-Ross, M.-D. Huang, H.-J. Heinrich, S. Recknagel, J. Vogl, N. Jakubowski and U. Panne, *Spectrochim. Acta Part B*, 2017, **136**, 116–122.

25 M. B. T. Zanatta, F. V. Nakadi, M. Resano and M. A. M. S. da Veiga, *J. Anal. At. Spectrom.*, 2019, **34**, 2280–2287.

26 J. Meija, T. B. Coplen, M. Berglund, W. A. Brand, P. De Bièvre, M. Gröning, N. E. Holden, J. Irrgeher, R. D. Loss, T. Walczyk and T. Prohaska, *Pure Appl. Chem.*, 2016, **88**, 293–306.

27 M. A. Elburg, Geochronological Dating, in *Isotopic Analysis: Fundamentals and Applications Using ICP-MS*, eds. F. Vanhaecke and P. Degryse, Wiley-VCH, Weinheim, 1st edn, 2012, pp. 235–274.

28 H. L. Whelton, J. Lewis, P. Halstead, V. Isaakidou, S. Triantaphyllou, V. Tzevelekidi, K. Kotsakis and R. P. Evershed, *J. Archaeol. Sci. Rep.*, 2018, **20**, 768–774.

29 K. J. Knudson, H. M. Williams, J. E. Buikstra, P. D. Tomczak, G. W. Gordon and A. D. Anbar, *J. Archaeol. Sci.*, 2010, **37**, 2352–2364.

30 N. Shalev, B. Lazar, L. Halicz, M. Stein, I. Gavrieli, A. Sandler and I. Segal, *Procedia Earth Planet. Sci.*, 2013, **7**, 790–793.

31 M. J. Kennedy, L. O. Hedin and L. A. Derry, *Proc. Natl. Acad. Sci. U.S.A.*, 2002, **99**, 9639–9644.

32 M. Tiwari, A. K. Singh and D. K. Sinha, Stable Isotopes: Tools for Understanding Past Climatic Conditions and Their Applications in Chemostratigraphy, in *Chemostratigraphy Concepts, Techniques, and Applications*, 1st edn, M. Rakumar, Elsevier, Amsterdam, 2015, pp. 65–92.

33 R. W. B. Pearse and A. G. Gaydon, *The identification of molecular spectra*, Chapman and Hall Ltd., London 4th edn, 1976.

34 G. Herzberg, in *Molecular Spectra and Molecule Structure I. Spectra of Diatomic Molecules*, D. Van Nostrand, New York, 2nd edn, 1950, p. 162.

35 A. A. Woolf, Thermochemistry of Inorganic Fluorine Compounds, in *Advances in Inorganic Chemistry and Radiochemistry*, vol 24, eds. H. J. Emeléus and A. G. Sharpe, Academic Press, New York, 1981, pp. 1–55.

36 B. Welz, F. G. Lepri, R. G. O. Araujo, S. L. C. Ferreira, M.-D. Huang, M. Okruss and H. Becker-Ross, *Anal. Chim. Acta*, 2009, **647**, 137–148.

37 D. J. Butcher, *Anal. Chim. Acta*, 2013, **804**, 1–15.

38 M. Resano, M. R. Flórez and E. García-Ruiz, *Anal. Bioanal. Chem.*, 2014, **406**, 2239–2259.

39 D. R. Lide, Ed., *CRC Handbook of Chemistry and Physics*, CRC Press, Boca Raton, 89th edn., 2008.

40 N. Ozbek and S. Akman, *Anal. Sci.*, 2013, **29**, 741–746.

41 M. Aramendía, M. R. Flórez, M. Piette, F. Vanhaecke and M. Resano, *J. Anal. At. Spectrom.*, 2011, **26**, 1964–1973.

42 N. Ozbek and S. Akman, *Spectrochim. Acta Part B*, 2012, **69**, 32–37.

43 X. Mao, A. A. Bol'shakov, I. Choi, C. P. McKay, D. L. Perry, O. Sorkhabi and R. E. Russo, *Spectrochim. Acta Part B*, 2011, **66**, 767–775.

Table 1. Sr isotopic atomic composition (in %) of all the enriched standards used in this work according to the certificate of analysis from the corresponding manufacturer.

Enriched isotope	Sr isotopic atomic composition (%)			
	^{84}Sr	^{86}Sr	^{87}Sr	^{88}Sr
^{84}Sr	75.5	4.4	2.0	18.1
^{86}Sr	0.003	95.21	1.15	3.69
^{87}Sr	< 0.005	0.8	90.8	8.4
^{88}Sr	< 0.01	0.02	0.08	99.9

Table 2. Optimized temperature program used to generate and monitor the SrF molecule with the gas-phase fluorinating agent (Ar/CH_3F). The actual parameters that were introduced in the instrument software for setting this program are included in **Table S2** of the ESI.

Step	Temperature (ºC)	Ramp (ºC s^{-1})	Hold (s)	Gas flow (L min^{-1})	
				Purge (Ar)	Ar/CH_3F
Drying	80	6	20	2	0
Drying	90	3	50	2	0
Drying	120	5	10	2	0
Pyrolysis	800	300	10	2	0
Gas adaption	800	0	6	0	0.5
Vaporization	2400	2000	5	0	0
Cleaning	2600	500	4	2	0

Table 3. Calculated isotopic shifts at different wavelengths for SrF molecule following equation (1). Characteristic masses experimentally determined for each wavelength, using the Ar/CH_3F gas mixture as fluorinating agent, are also indicated, as well as the experimentally observed resolution of the spectrometer at the transition wavelength.

Wavelength (nm)	Calculated isotopic shift (pm)			Characteristic mass (μg)	Resolution (pm pixel^{-1})
	^{87}Sr-^{88}Sr	^{86}Sr-^{88}Sr	^{84}Sr-^{88}Sr		
641.76	21.0	42.4	86.6	0.045	5.0
639.47	20.8	42.1	85.9	<LOD	3.8
630.34	20.3	40.9	83.5	0.031	4.6
628.31	20.1	40.6	83.0	<LOD	4.7
567.00	15.6	31.5	64.3	<LOD	4.3
372.16	7.3	14.7	29.9	0.22	2.4
364.10	6.9	14.0	28.6	0.14	2.6
345.72	8.0	16.2	33.0	<LOD	2.2
292.96	11.1	22.4	45.8	<LOD	1.8

Table 4. 95% confidence intervals (n = 5) for the slope and intercept of the regression lines obtained when plotting the absorbance ratio against the molar ratio of the different Sr isotopes, as shown in **Figure 8**.

Isotope ratio	Before correction		After correction	
	Slope	Intercept	Slope	Intercept
$^{87}Sr/^{88}Sr$	0.94 ± 0.12	0.02 ± 0.07	0.94 ± 0.12	0.02 ± 0.07
$^{88}Sr/^{86}Sr$	0.82 ± 0.16	0.03 ± 0.07	0.97 ± 0.09	0.01 ± 0.04
$^{84}Sr/^{88}Sr$	0.94 ± 0.06	0.02 ± 0.03	0.96 ± 0.05	0.00 ± 0.03

Table 5. Isotopic ratios determined for different concentrations of naturally abundant strontium standards. Experimental results are compared with the values calculated from the theoretical natural abundances[17] with a Student's t-test, leading to the collected P_0 values that indicate the probability of data not being significantly different. Uncertainties are expressed as standard deviation (n = 3).

Total Sr concentration	$^{87}Sr/^{88}Sr$ ratio		
	Experimental	Theoretical	P_0
100 mg L^{-1}	0.080 ± 0.005	0.085	0.22
200 mg L^{-1}	0.089 ± 0.008	0.085	0.45
Total Sr concentration	$^{86}Sr/^{88}Sr$ ratio		
	Experimental	Theoretical	P_0
100 mg L^{-1}	0.115 ± 0.008	0.119	0.47
200 mg L^{-1}	0.112 ± 0.012	0.119	0.40

Table 6. Isotopic ratios determined for a solution prepared from the dilution and mixing of monoisotopic standards. Experimental results are compared with the theoretical values applying a Student's t-test, leading to the resulting P_0 values. Uncertainties expressed as standard deviation (n = 5).

Isotope ratio	Experimental ratio	Theoretical ratio	P_0
$^{87}Sr/^{88}Sr$	0.601 ± 0.038	0.642	0.07
$^{86}Sr/^{88}Sr$	0.659 ± 0.049	0.701	0.09
$^{84}Sr/^{88}Sr$	0.364 ± 0.028	0.393	0.08

Table 7. Isotopic concentrations determined for a tap water sample by both HR CS GFMAS and ICP-MS, after spiking it. Results are compared applying a Student's t-test, leading to the resulting P_0 values. Uncertainties expressed as standard deviation (n = 5)

Isotope	Experimental concentration (mg L^{-1})		
	HR CS GFMAS	ICP-MS	P_0
^{84}Sr	55.65 ± 6.81	57.72 ± 0.30	0.94
^{88}Sr	13.58 ± 1.63	11.71 ± 0.13	0.06

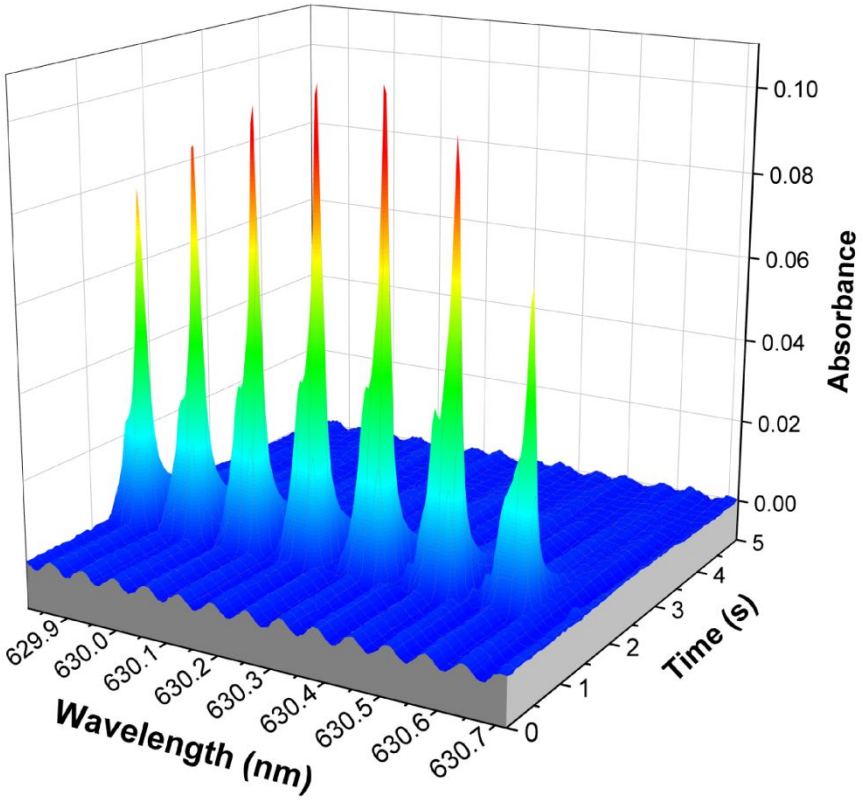

Figure 1. SrF spectrum registered for 10 µL of a 10 mg L^{-1} strontium solution of natural abundance, using the temperature program included in **Table 2**. The central pixel of the spectrometer was fixed at 630.27 nm.

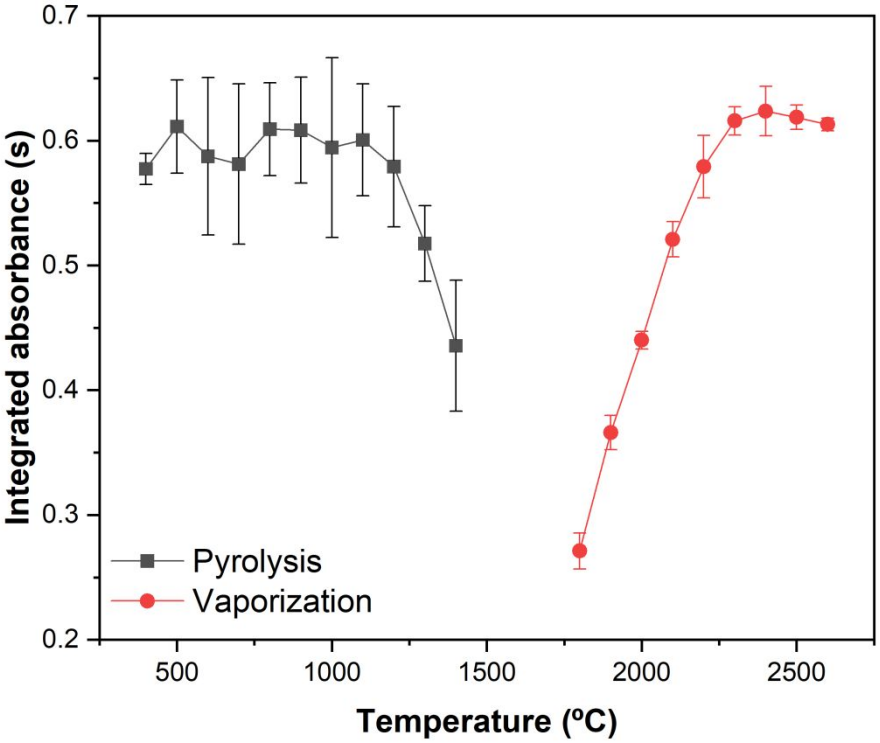

Figure 2. Optimization of the pyrolysis and vaporization temperatures to monitor SrF by HR CS GFMAS for 10 µL of a 10 mg L^{-1} solution of naturally abundant Sr. A pyrolisis temperature of 800 ºC was set for the vaporization study, and a vaporization temperature of 2400 ºC for the pyrolisis study. The three central pixels of the transition at 651.187 nm were summed for quantitation. Error bars represent the standard deviation (n = 3)

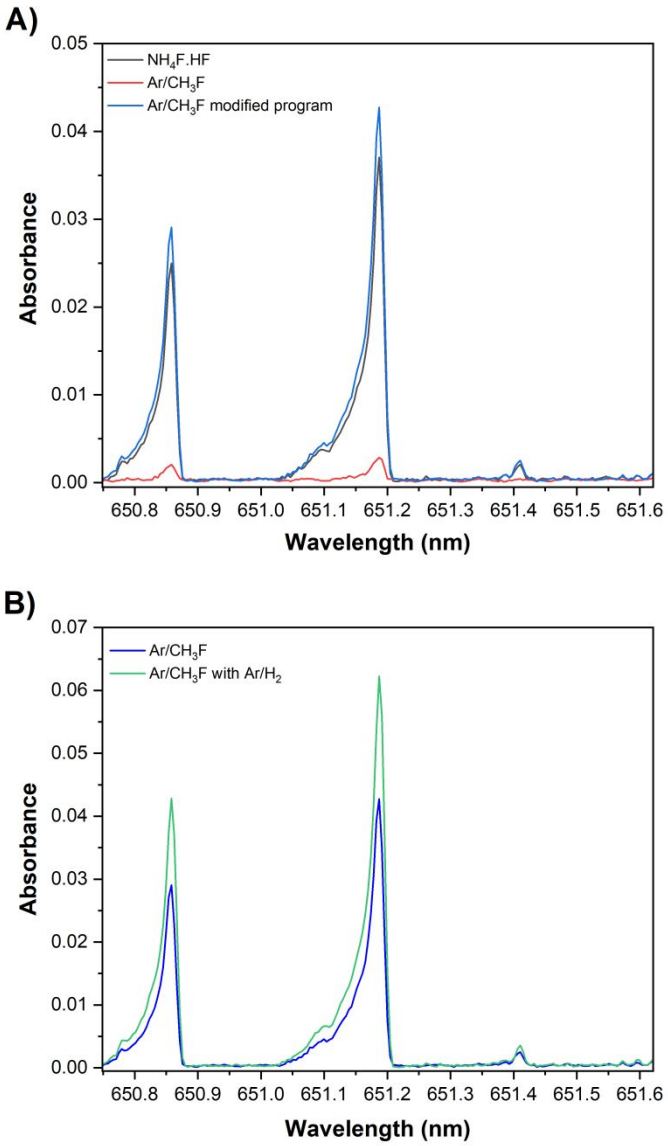

Figure 3. Spectra registered at the vicinity of 651.187 nm for 10 µL of a standard solution of 100 µg L^{-1} in naturally abundant strontium for (A) different fluorinating agents: 10 µL of $NH_4F{\cdot}HF$ 5% m/m (black line) and 0.5 L min^{-1} of Ar/CH_3F (red line) using the temperature program of **Table S1**, and 0.5 L min^{-1} of Ar/CH_3F (blue line) using the temperature program of **Table 2.** The presence (green line) and absence (blue line) of H_2 in the purge gas flow (B) was also evaluated.

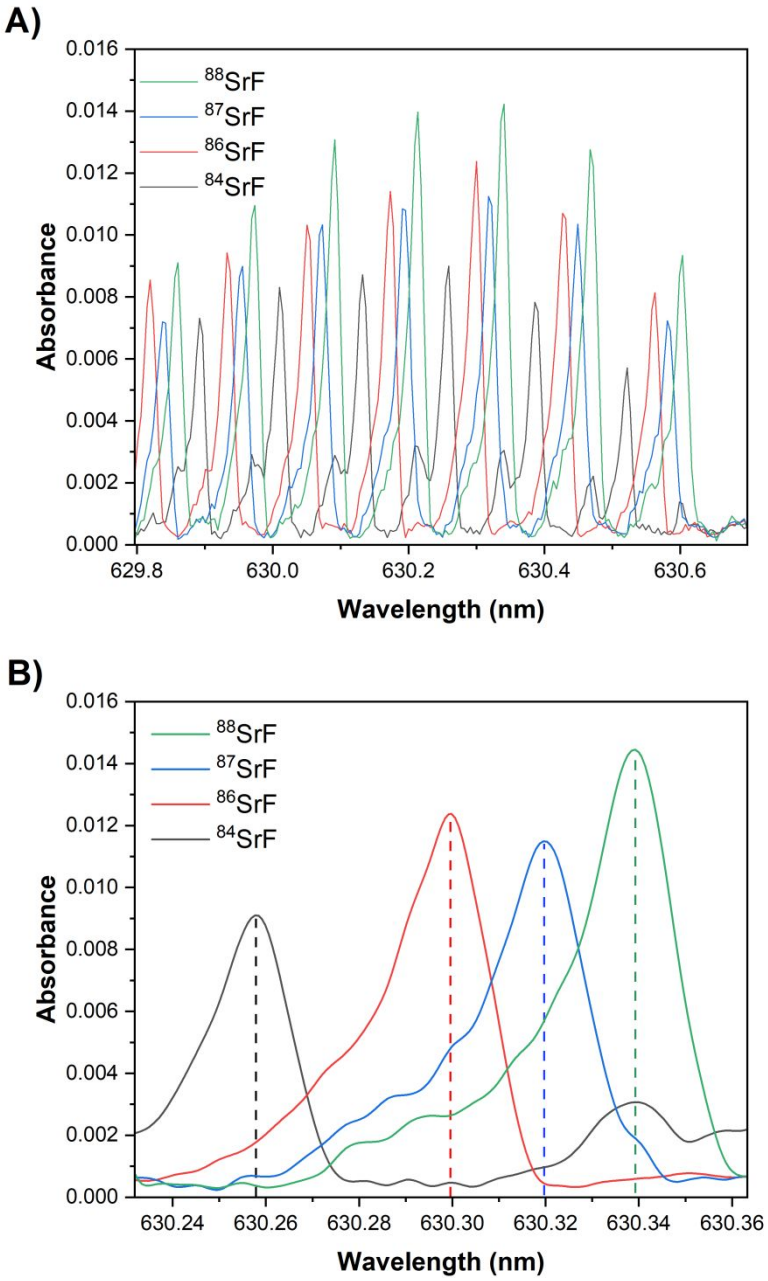

Figure 4. Stacked spectra obtained for the different Sr enriched isotopic standards (10 µL of a 10 mg L^{-1} Sr solution was measured for each standard). The entire spectral window (**A**) or the most sensitive band (**B**) is shown. Dashed lines indicate the wavelength at which the maximum of each isotope is observed.

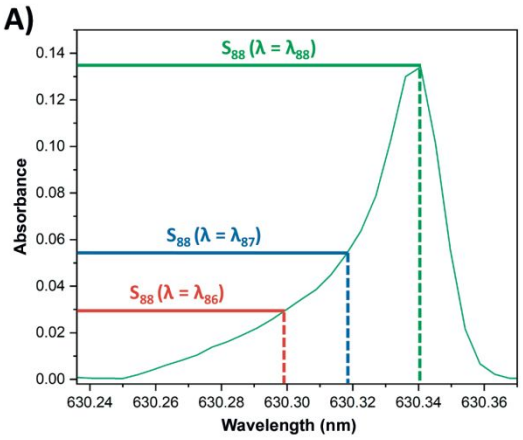

B)

Signal ratio	Determination	Value
$R_{88,87} = R_{87,86}$	$\frac{S_{88}(\lambda = \lambda_{87})}{S_{88}(\lambda = \lambda_{88})}$	0.391 ± 0.014
$R_{88,86} = R_{86,84}$	$\frac{S_{88}(\lambda = \lambda_{86})}{S_{88}(\lambda = \lambda_{88})}$	0.219 ± 0.008

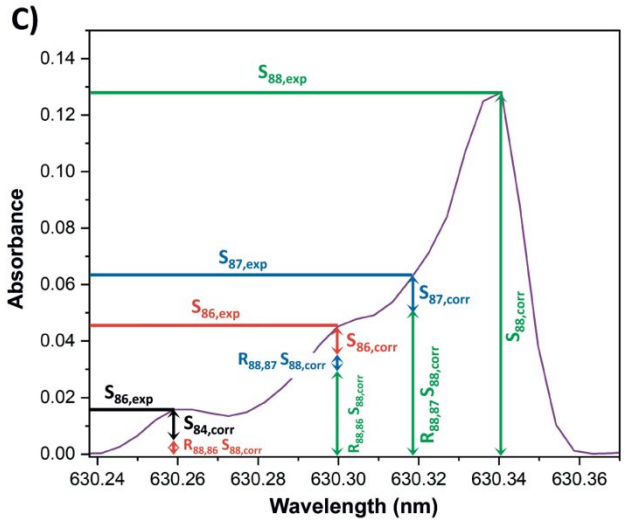

Figure 5. Representation of the correction protocol for the spectral overlap. It consists of the obtention of the signals registered for the profile of 10 µL of an 80 mg L^{-1} ^{88}Sr-enriched standard at the wavelengths where the maximum of each Sr isotope is expected (A). From such signals, the correction ratios are calculated and extrapolated to other isotopes of lesser pure standards (B). Once the ratios are calculated, the corrected signals for every isotope can finally be determined from the non-monoisotopic spectra, according to equation (2) (C).

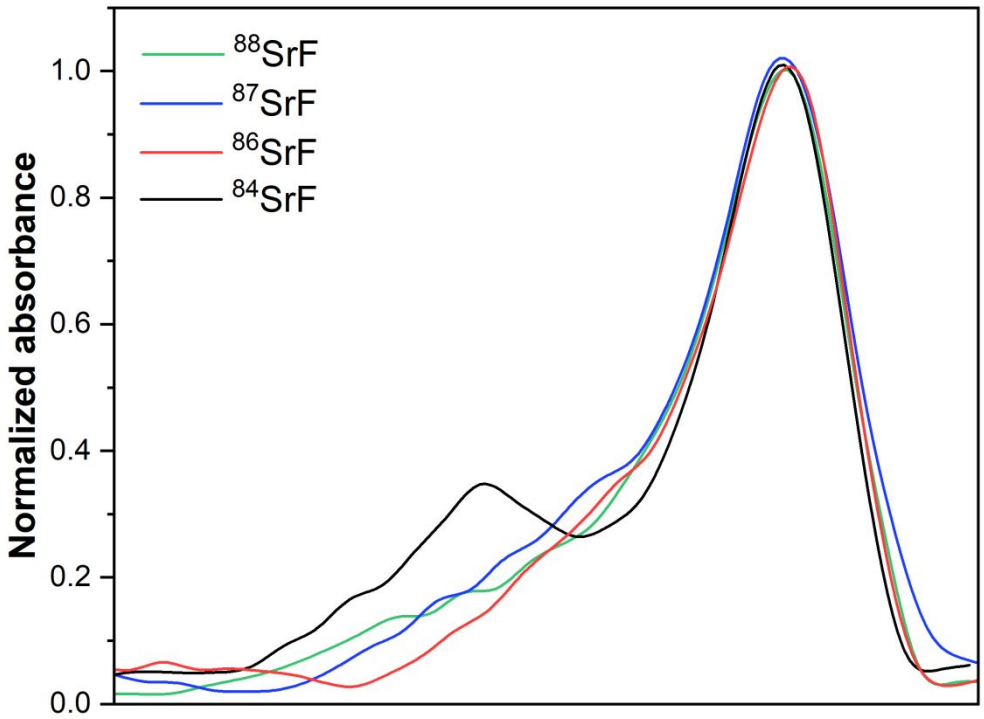

Figure 6. Normalized and shifted wavelength-resolved absorbance peaks of SrF obtained for each monoisotopic standard at the most sensitive band.

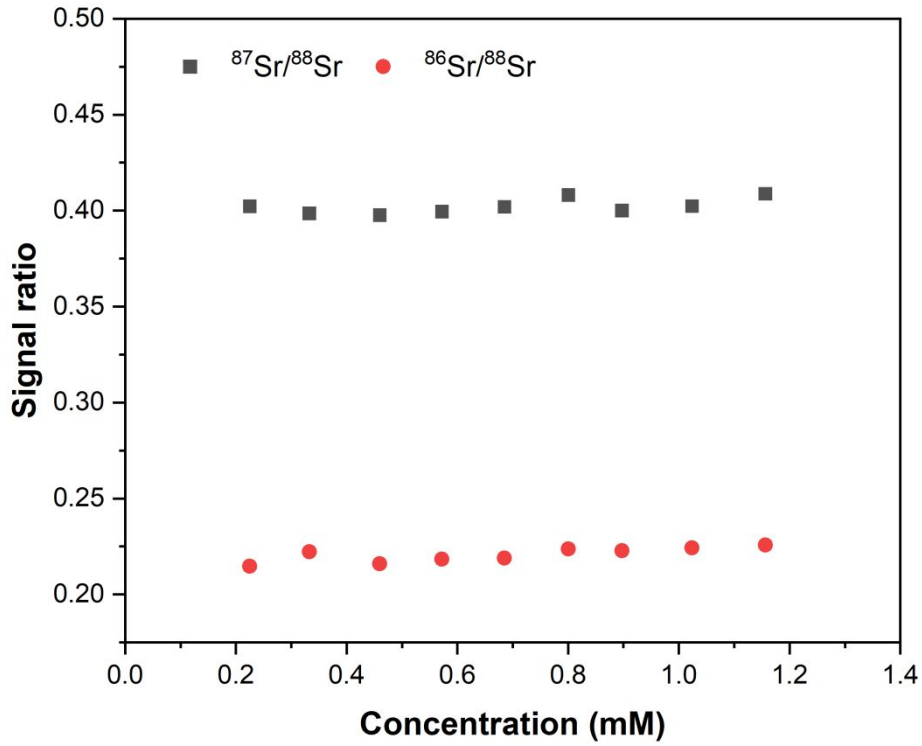

Figure 7. Evolution of $^{87}Sr/^{88}Sr$ and $^{86}Sr/^{88}Sr$ correction ratios observed when increasing the concentration of ^{88}Sr.

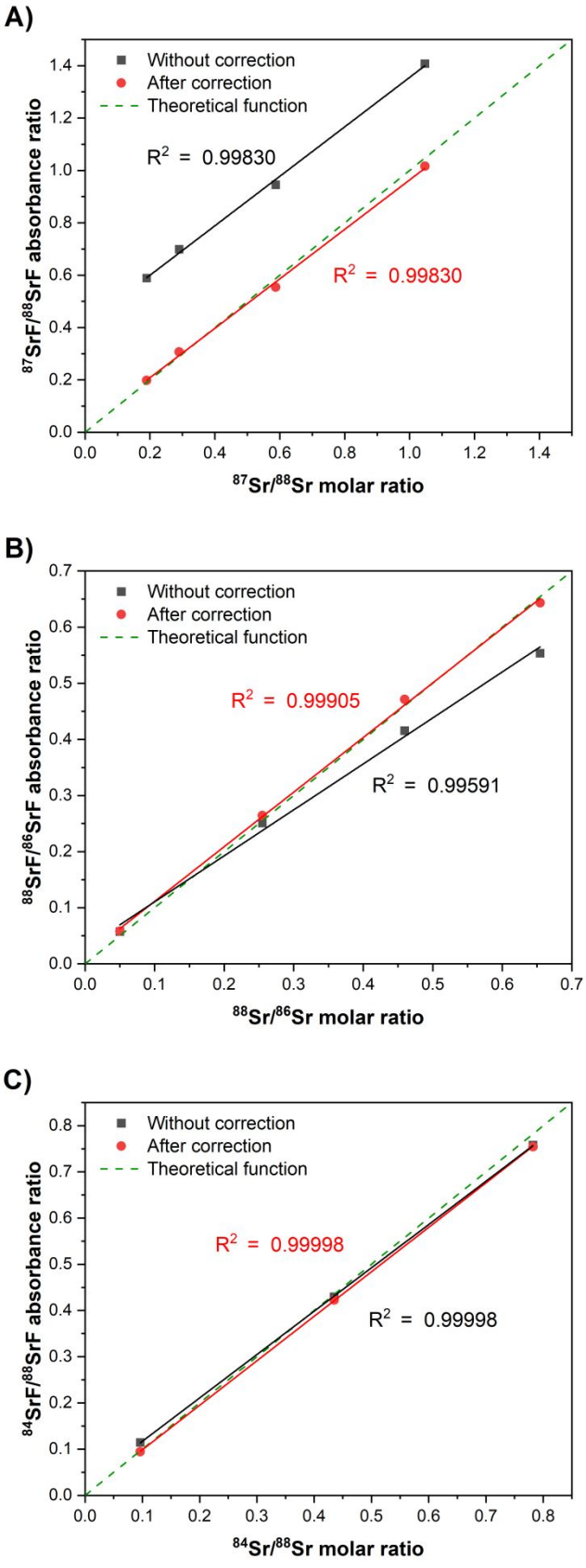
A)
Without correction
After correction
Theoretical function
R² = 0.99830
R² = 0.99830
87SrF/88SrF absorbance ratio
87Sr/88Sr molar ratio
B)
Without correction
After correction
Theoretical function
R² = 0.99905
R² = 0.99591
88SrF/86SrF absorbance ratio
88Sr/86Sr molar ratio
C)
Without correction
After correction
Theoretical function
R² = 0.99998
R² = 0.99998
84SrF/88SrF absorbance ratio
84Sr/88Sr molar ratio

Figure 8. Correlation between the experimental (as obtained *via* HR CS GFMAS by monitoring SrF), corrected, and theoretical values for $^{87}Sr/^{88}Sr$ (**A**), $^{87}Sr/^{88}Sr$ (**B**), and $^{84}Sr/^{88}Sr$ (**C**) as obtained for a set of solutions prepared by mixing different amounts of a Sr standard of natural abundance and of isotopically enriched Sr standards.

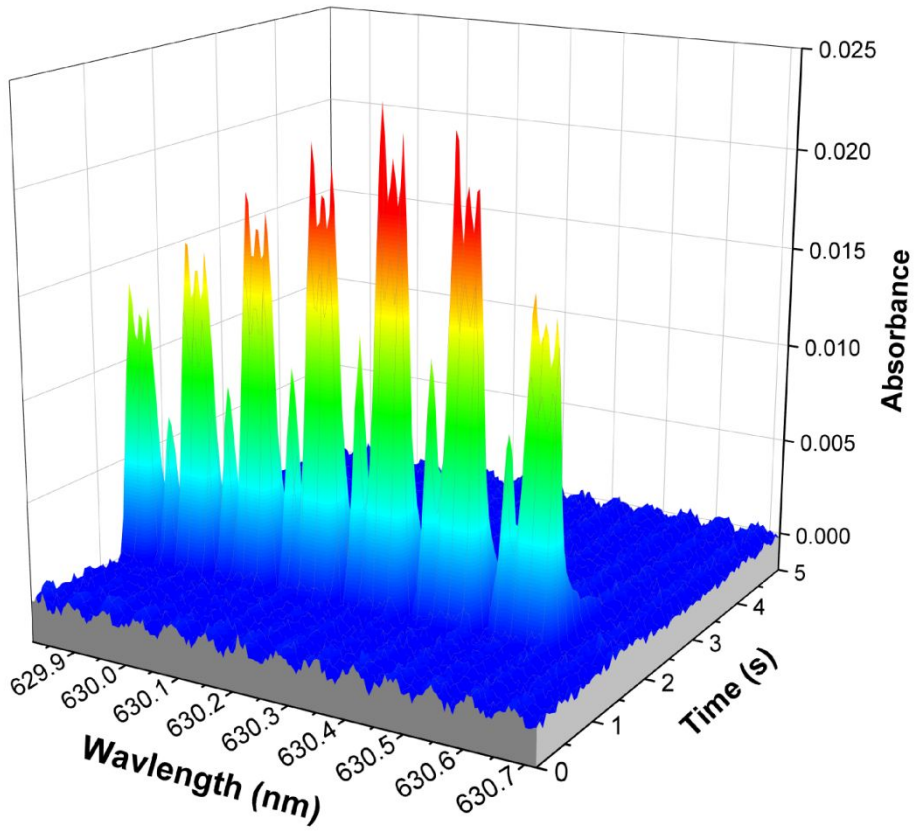

Figure 9. Experimental spectrum registered for 20 µL of a standard prepared with a concentration of 0.12 mM in total strontium for each isotope-enriched standard. The central pixel was placed at 630.27 nm.